New Journal of Physics
The open-access journal for physics

TAMR effect in (Ga,Mn)As-based tunnel structures

M Ciorga, M Schlapps, A Einwanger, S Geißler, J Sadowski[1], W Wegscheider and D Weiss[2]

Institute for Experimental and Applied Physics, Regensburg University, 93040 Regensburg, Germany
E-mail: dieter.weiss@physik.uni-regensburg.de

New Journal of Physics **9** (2007) 351
Received 9 May 2007
Published 28 September 2007
Online at http://www.njp.org/
doi:10.1088/1367-2630/9/9/351

Abstract. We discuss the results of our experiments on tunnel devices based on (Ga,Mn)As structures. Those include p^+-(Ga, Mn)As/n^+-GaAs Esaki diodes and laterally defined narrow nanoconstrictions in (Ga,Mn)As epilayers. We found in those structures strong anisotropic magnetoresistance behaviour with features that could be attributed to the novel tunnelling anisotropic magnetoresistance effect. We argue however, that in case of nanoconstricted (Ga,Mn)As wires, some other physics has to be additionally employed to fully explain the observed effects.

[1] Present address: MAX-Laboratory, Lund University, SE-221 00, Lund, Sweden.
[2] Author to whom any correspondence should be addressed.

PII: S1367-2630(07)50091-1

Contents

1. Introduction

III–V materials belong to the most widely used semiconductors. The discovery of ferromagnetism in the family of (III,Mn)V materials opened new routes into successful combination of magnetism and semiconductor physics in the field of semiconductor spintronics and offered possibilities of new devices. Numerous studies of (III,Mn)V semiconductors, especially (Ga,Mn)As, followed, resulting in discovery of many interesting magneto-semiconducting properties. One of these novel spintronic phenomena is tunnelling anisotropic magnetoresistance (TAMR) discovered by Gould *et al* [1] in experiments involving tunnelling from a gold layer into a single (Ga,Mn)As layer through a thin barrier made of aluminium oxide. The magnetoresistance measured in their structure was found to be dependent on the angle between the magnetization and crystallographic axes. This effect arises due to anisotropies in (Ga,Mn)As density of states with respect to magnetic moment **M**, because of a strong spin–orbit coupling. Combined with the two-step magnetic reversal processes [2, 3], this resulted in a spin-valve-like behaviour with the signal amplitude in the order of ∼3%. In a two-layer tunnelling magnetic junction (TMJ) (Ga,Mn)As/GaAs/(Ga,Mn)As [4] this effect lead to a huge spin-valve signal ∼100 000% at $T = 1.7$ K. In that case, the metal–insulator transition picture was postulated as a possible origin of the enhancement of the TAMR effect in a 10 nm thick (Ga,Mn)As injector layer. The effect was also observed in the other tunnelling devices with ferromagnetic contacts. There has been an experimental report on the TAMR effect in a (Ga, Mn)As/n^+-GaAs Zener–Esaki diode in a perpendicular magnetic field configuration [5]. Moser *et al* [6] observed TAMR in an Fe/GaAs/Au tunnel junction, i.e. with a traditional magnetic metal contact. The existence of the effect is, however, not limited to vertical tunnelling devices. Giddings *et al* [7] reported on the large TAMR observed in a single (Ga,Mn)As epilayer in tunnel transport through laterally defined nanoconstrictions. The importance of the TAMR effect lies in the fact that the spin-valve-like behaviour can be observed in structures with only one magnetic layer. This could offer new possibilities for operating spintronic devices. From the other side, this effect should be taken into account while interpreting the results of spin-injection experiments in a spin-valve configuration.

In this paper, we discuss our experiments on different (Ga,Mn)As-based tunnel structures, in which we observed magnetoresistance effects, that we attribute to the TAMR effect. In the next section, we discuss the results of our studies on p^+-(Ga, Mn)As/n^+-GaAs Esaki diode devices. We find that the observed spin-valve signal strongly depends on the underlying magnetic anisotropy of the magnetic layer. We distinguish three different types of anisotropy depending on the direction of the uniaxial anisotropy superimposed on the dominant biaxial cubic anisotropy: (I) along biaxial easy axes, (II) along biaxial hard axes or (III) along both of them. The type of the anisotropy present in the device is found to be strongly shaped, in a random way, during processing of the wafer. Samples with uniaxial anisotropy along the biaxial easy axes (types I and III) show sign reversal of the spin-valve signal upon rotation by 90° in an in-plane magnetic field, as for the samples investigated in [1]. This way a TAMR-related signal could be distinguished from a *real* spin-valve signal involving two-magnetic layers. This is not the case however for all the samples. Some of them, with a different type of anisotropy, do not show the sign reversal. This could then make the interpretation of the results of the possible spin-injection experiments more difficult.

In the second part, we focus on the experiments on tunnel devices with small nano-constrictions in (Ga,Mn)As epilayers. We observe strong magnetoresistance effects with many features characteristic for the TAMR effect, namely sign reversal of the spin-valve signal upon rotation in an in-plane magnetic field. The size of the observed effect and more detailed analysis of the experimental data suggest, however, that some additional physics has to be employed to fully explain the behaviour of these nanostructures in a magnetic field.

2. TAMR in p^+-(Ga, Mn)As/n^+-GaAs Esaki diode devices

2.1. Introduction

Ferromagnetic (Ga,Mn)As is a very good candidate for an injector of spin-polarized carriers into a non-magnetic semiconducting material because of its high spin polarization, as well as its high quality heterojunction with GaAs. Its p-type character determines, however, that any direct injection would result in spin-polarized holes, characterized by short spin relaxation times. This problem has been circumvented by employing (Ga,Mn)As/GaAs Esaki–Zener tunnel junctions. It has been demonstrated that in such devices the injection of spin-polarized electrons can be achieved through interband tunnelling of spin-polarized electrons from the valence band in (Ga,Mn)As into the conduction band of GaAs [8] under reverse bias applied to the junction. Recent experiments showed very high (∼80%) spin polarization obtained in such structures [9]. To date, all the experiments on (Ga,Mn)As/GaAs Esaki–Zener tunnel junctions employed the optical detection of spin polarization. Spin valve experiments with Esaki diodes as injectors/detectors are still to be realized. Observation of a TAMR effect in different tunnelling (Ga,Mn)As devices made it necessary also to take this effect into account in the above mentioned possible spin-injection experiments. According to recent theoretical work [10], the presence of the TAMR effect with a strength of several percent is expected in such devices, both for the in-plane and out-of-plane magnetization. The only experimental work so far, according to our knowledge, regarded the latter case [5]. We have already reported on our preliminary experiments on (Ga,Mn)As/GaAs Esaki devices in an in-plane configuration [11]. Here, we summarize and discuss the results of all our experiments.

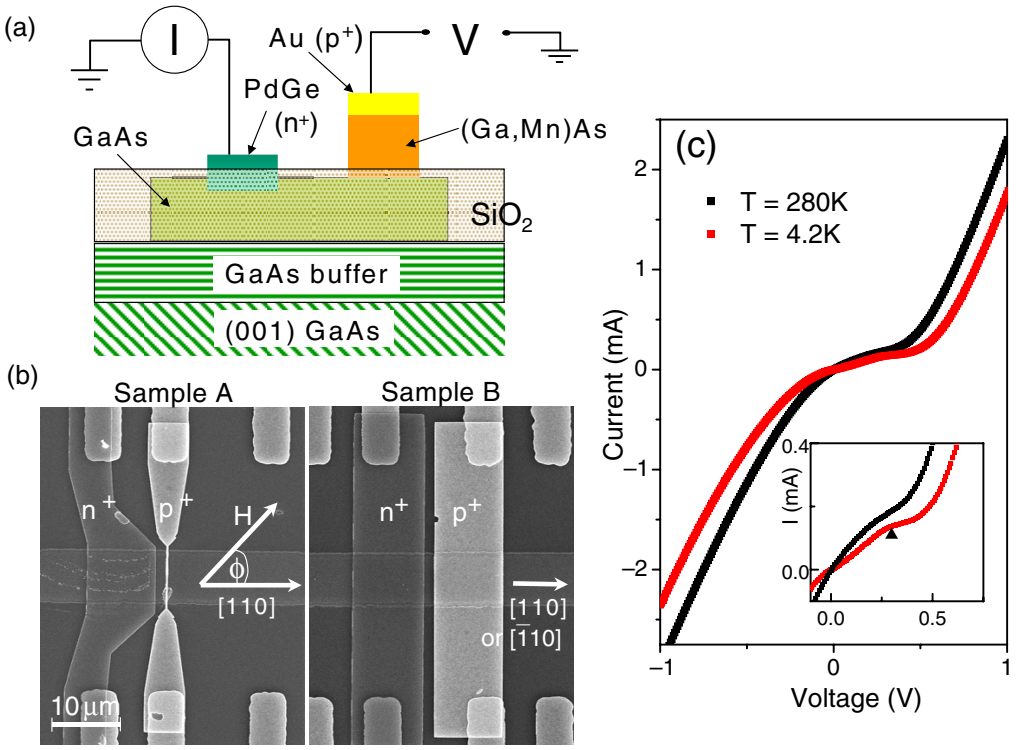

Figure 1. (a) Schematics of the Esaki diode device; (b) SEM pictures of devices similar to those measured; (c) typical (sample B) current–voltage (I–V) characteristics of the measured devices taken at 280 K (black) and 4.2 K (red). Inset: I–V characteristics in the smaller voltage range; the region of slightly suppressed conductance in the forward bias, characteristic for Esaki tunnel devices, is marked by the black triangle.

2.2. Experimental details

2.2.1. Sample preparation. All devices were structured on the same molecular beam epitaxy (MBE)-grown wafer. We focus here on the data from the two devices, which we name A and B. The Esaki diode structure consists of a 100 nm thick magnetic (Ga,Mn)As layer, with Mn content of 4.5%, grown by a low-temperature (LT) MBE at $T \approx 260$ K on 100 nm n^+-doped ($\sim 10^{19}$ cm^{-3}) GaAs. This structure was grown on GaAs (001) substrate with 160 nm GaAs buffer in between. The wafer was then processed into proper devices. The schematic of the device is shown in figure 1(a). Mesas 10 μm wide and 100 μm long, directed along one of the [110] directions, were defined using optical lithography and wet chemical etching. An SiO_2 layer was then deposited around mesas to avoid an unwanted electrical contact between n^+ and p^+ layers at the sides of the mesa. In the next step, electron beam lithography was used to define Au contacts to the (Ga,Mn)As layer. Evaporated gold was then used as an etching mask for the reactive ion etching (RIE) employed to structure the Esaki diode device. Finally, electrical contacts to n^+-GaAs were defined by e-beam lithography followed by the evaporation of PdGe alloy and 5 min of annealing at 250 °C. The scanning electron microscope (SEM) pictures of exemplary devices are shown in figure 1(b). In sample B, the p^+ magnetic contact is $10 \times 10\ \mu$m^2, whereas sample A features a p^+ contact of $0.2 \times 10\ \mu$m^2 size with its long side oriented along the [$\bar{1}$10] direction.

2.2.2. Magnetotransport measurements. The samples were mounted in a ^{4}He bath cryostat on the holder enabling in-plane rotation of the sample in an applied magnetic field. The results discussed here are for the fields in the plane of the magnetic layer with the field direction given by the angle ϕ with respect to the mesas long axis, as indicated in figure 1(b). For sample A, it is a [110] direction whereas for sample B it is either [110] or [$\bar{1}$10] (the exact orientation is not known). Two types of measurement scans were performed. In the *angle scan*, the value of an external magnetic field **H** was kept constant while the sample was rotated, i.e. the angle ϕ was changed. In the *field scans*, this angle was fixed and the magnetic field was swept from the saturation in one magnetic field direction to saturation in the opposite direction. All magnetotransport measurements were performed using an ac lock-in technique by applying an excitation voltage of 1 mV at a frequency of 17 Hz to the (Ga,Mn)As contact and measuring the resulting current at the GaAs contact. The temperature of measurements was 4.2 K.

2.3. Results and discussion

Figure 2 shows angle scans performed for the discussed devices at an external magnetic field **H** of 1 and 0.1 T. A TAMR effect results in gradual changes in magnetoresistance, plotted normalized to its highest value, as the sample is rotated in an in-plane magnetic field. The value of 1 T is big enough to rotate the magnetization away from an easy axis and orient it along **H**. In the TAMR picture, the measured resistance is related to the density of states in the (Ga,Mn)As layer and its dependence on the magnetization direction. The resulting scans reflect then, to a certain degree, the symmetry of the crystal structure of the (Ga,Mn)As device. The observed symmetry breaking between the different crystal directions could be expected also in the magnetic anisotropy. Although in our experiment, we did not measure directly the magnetic anisotropy of the samples (how it could be done with magnetotransport techniques is described e.g. in [12]), we could use the low magnetic field data to identify the hard and easy magnetic directions. For sample A that was easily achieved with the angle scans at 0.1 T. As this field value is not strong enough to align **M** along **H**, the former prefers to stay longer in the vicinity of easy axes. Following this argument, one can then deduce from figure 2(a) that in the case of sample A the easy axes lie along [100] directions, which is a commonly reported observation for (Ga,Mn)As layers [1, 14, 15]. It is then worth noting that higher resistance values correspond to easy axes whereas low resistance is measured when **M** aligns along a hard axis. This magnetic anisotropy–transport anisotropy correspondence is in contrast to the main data of Gould *et al* [1], where high/low resistance values correspond to hard/easy magnetic axes. One has to keep in mind however, that transport and magnetic anisotropies can vary independently in the system, as also was proved in [1]. Let us assume for the moment that this correspondence is valid also for sample B at the saturation field of 1 T. Although the direction of easy and hard axes in this sample cannot be clearly deduced from the 0.1 T scan, we will prove that this is really the case later after detailed discussion of the respective field scans. In further discussion, by ‘anisotropy (symmetry) type’, we mean anisotropy (symmetry) observed in an angular scan at 1 T with hard/easy magnetic directions identified from low-field measurements: 0.1 T angle scan for sample A and field scans for sample B.

The scans in figure 2 then reveal three distinct types of anisotropy observed in our samples. The common feature in these scans is a dominant four-fold symmetry, characteristic for a cubic anisotropy. The strength of related TAMR, taken as a ratio of maximum to minimum resistance, is in the order of ∼2–2.5%. All samples also show a uniaxial anisotropy characterized by a

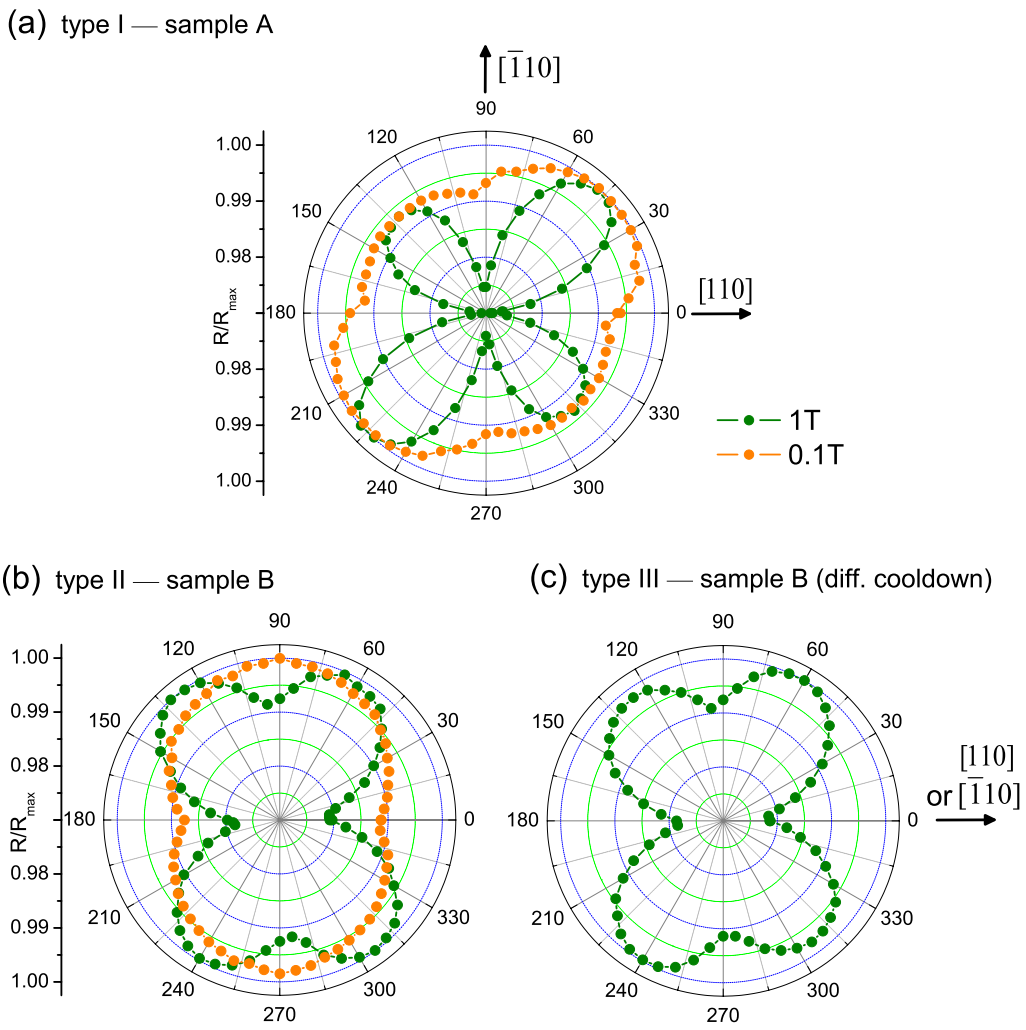

Figure 2. Angle scans in the constant field **H** of 1 T (green) and 0.1 T (orange) illustrating the three discussed types of anisotropy with the uniaxial anisotropy superimposed on (a) easy axes; (b) hard axes and (c) both easy and hard axes of a biaxial cubic anisotropy.

two-fold symmetry. For all of the measured samples, it is superimposed on the hard cubic axes [110], and [1̄10] with the related TAMR strength ∼0.5%. Its direction and strength changes however for some samples, and this is where the difference between the three discussed types of anisotropy lies. The positions of the main axes of uniaxial and cubic anisotropy in each of the three types are sketched schematically in figure 3(a).

The type I, observed for sample A, features a two-fold uniaxial symmetry superimposed on [100] cubic easy axes, with high and low resistance along [010] and [100] directions, respectively, as seen in figure 2(a). The strength of related TAMR effect in this case is ∼0.7%. The type II, observed for sample B (figure 2(b)), is characterized by a much stronger uniaxial anisotropy superimposed on cubic hard directions. Its strength is 1.3%, given by the ratio of the resistance along the 90° direction (high-resistance (HR) uniaxial axis) to the resistance along the 0° direction (low-resistance (LR) uniaxial axis). As a result of this uniaxial anisotropy,

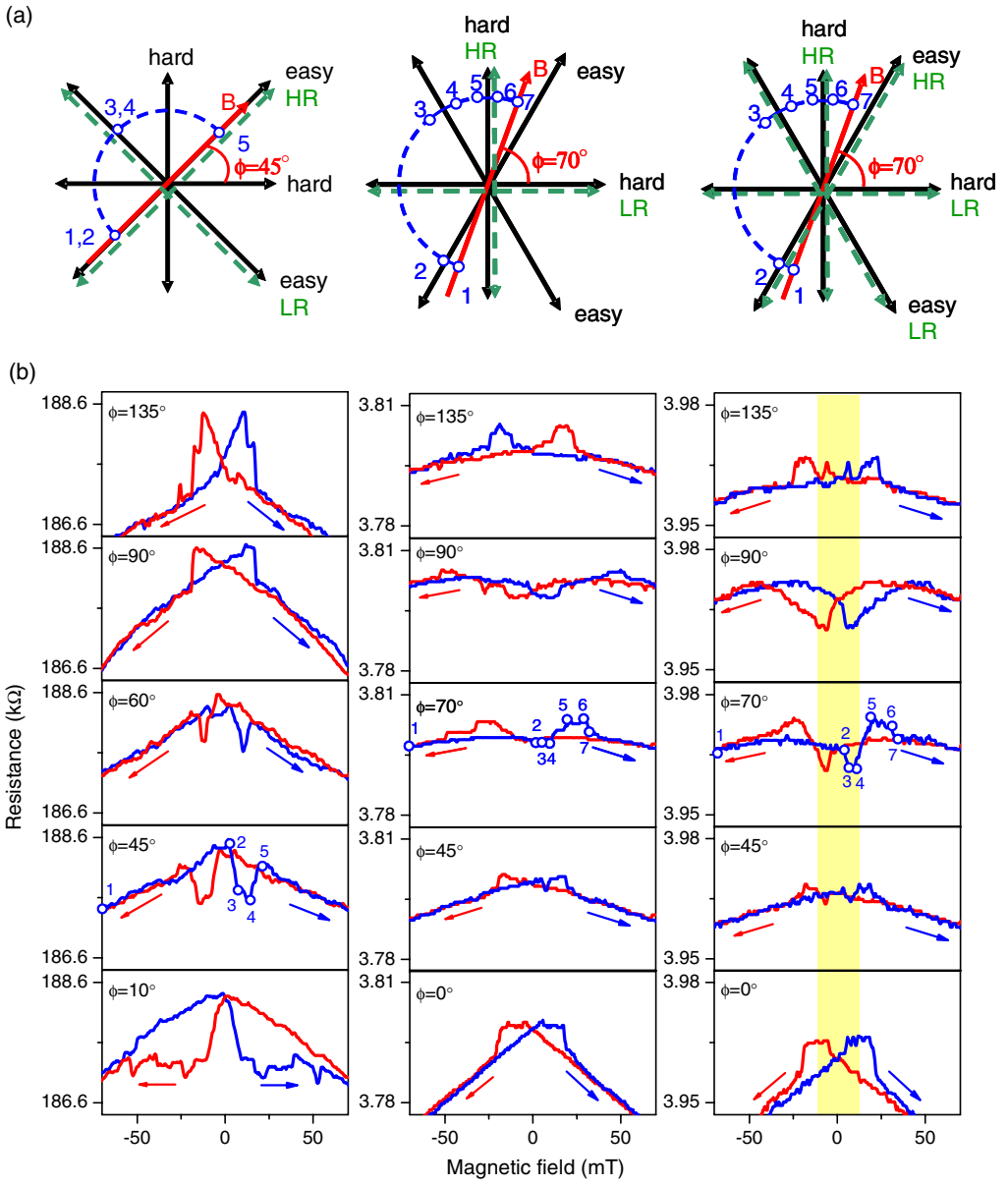

Figure 3. (a) Schematic representation of three types of anisotropies discussed in the text: type I (leftmost panel), type II (middle panel) and type III (rightmost panel). Hard and easy axes of biaxial (black colour) anisotropy are indicated. The main axes of uniaxial (green) anisotropy are labelled as HR and LR directions, as measured at $B = 1\,\mathrm{T}$. (b) Magnetic field scans at different angles ϕ between magnetic field and mesas long axis for samples A (the leftmost panel) and B (the middle and the rightmost panel) characterized by anisotropy types presented in (a). Magnetic field was swept between $-1\,\mathrm{T}$ and $+1\,\mathrm{T}$ in both the positive and negative direction. The possible magnetization reversal process for a chosen fixed angle for each anisotropy type is shown also in (a). For details see the text.

global easy axes are no longer along [100] directions but are drawn by about 15° towards the uniaxial HR axis (the middle panel of figure 3(a)). The type III was observed also for sample B (figure 2(c)) but on a different cooldown. One can see in this case, a small (∼0.5%) but clear difference in resistance along both the biaxial easy axes, suggesting the presence of an additional uniaxial anisotropy. This type can be then described as the combination of the type I and II, as the uniaxial anisotropy is superimposed on *both* easy and hard cubic axes (the rightmost panel of figure 3(a)).

The type of anisotropy strongly affects the spin-valve-like signal observed in field scans performed at different angles ϕ. The scans are shown in figure 3(b). The magnetic reversal processes lead in all cases to the spin-valve-like effect with the amplitude of ∼0.3%. Sample A (the leftmost panel), exhibiting type I anisotropy, shows similar switching pattern to the sample investigated by Gould *et al* [1]. We can see at $\mathbf{H} = 0$ two distinct levels with different resistance: high (∼188.5 kΩ) for $0°(180°) < \phi < 90°(270°)$ and low (∼187.6 kΩ) for $90°(270°) < \phi < 180°(360°)$. This is the result of the additional uniaxial anisotropy breaking the equivalency of the global easy axes. The sign of a spin-valve signal is then negative (positive), i.e. the resistance outside the switching fields is higher (lower) than between, in the former (latter) case (the exceptions are scans for $\alpha = 0°$ and 90°, i.e. along the cubic hard axes). The sign then switches every 90°. The magnetic reversal process is schematically shown in the leftmost panel of figure 3(a) for the angle $\phi = 45°$, i.e. for **H** applied along the easy biaxial and high resistance (HR) uniaxial axis (*easy/HR* axis in figure 3(a)). At the position 1, **H** is big enough so **M** is aligned along the $[0\bar{1}0]$ direction. When the magnitude of the field is decreased, **M** remains aligned along this axis as this is the global easy axis. The resistance change in the 1–2 region is due to an additional 'background' magnetoresistance observed in case of sample A and independent of the angle α. The origin of this signal is not known and not discussed here. At a certain value of **H** (point 2) **M** switches from the $[0\bar{1}0]$ axis to the global easy axis located 90°askew from this one (position 3). In the region 3–4, **M** is then aligned along the $[\bar{1}00]$ axis. Because this is the uniaxial LR axis (see figure 2(a)) the measured signal drops. At a certain value of **H** (position 4) **M** completes its reversal rotating by a further 90° and aligning again along the easy/HR [010] axis. Such a two-step reversal process can be explained by a nucleation and propagation of a 90° domain wall [1–3].

Let us now discuss the behaviour of the spin-valve-like signals observed for sample B when it is characterized with either anisotropy type II or III. We compare related field scans, shown respectively in the middle and the rightmost panel of figure 3(b), to discuss their differences and similarities in connection with the angle scans shown in figures 2(b) and (c). The first big difference that can be noted from the scans is the value of resistance at $\mathbf{H} = 0$ T. In the case of the type II, this resistance is independent of the direction of the applied field, whereas for the type III two distinct levels of resistance appear at $\mathbf{H} = 0$: high (∼3.967 kΩ) for $0°(180°) < \phi < 90°(270°)$ and low (∼3.96 kΩ) for $90°(270°) < \phi < 180°(360°)$. Please note here, that the latter behaviour is similar to that observed for sample A, i.e. anisotropy type I. This also suggests in this case, the existence of the two global easy axes with their equivalence broken by the additional uniaxial anisotropy. For the detailed discussion of the reversal process, we have chosen scans for **H** applied at the angle $\phi = 70°$. The schematics of the process is shown for both discussed cases, i.e. the types II and III, in the middle and the rightmost panel of figure 3(a), respectively. For a big enough magnetic field (position 1) **M** aligns along the direction of **H**. When the latter approaches zero, **M** aligns along the easy biaxial axis closest to the initial **H** direction (position 2). After reversing the sign of **H**, at a certain value **M**

switches its direction and aligns along the other easy biaxial axis (position 3). For the type III anisotropy, it is reflected in the spin-valve signal because of the additional uniaxial anisotropy along those axes: the resistance drops as **M** switches from easy/HR to easy/LR axis (step 2–3). In the range 3–4, **M** stays aligned along the easy/LR axis and then, during step 4–5, it moves towards the hard/HR axis and the measured resistance increases. It stays there during the 5–6 step and then, at higher field values becomes aligned along the direction of **H** and the reversal is completed. One can then see that in the case of the type III, the observed spin-valve-like signal can be described as a combination of two independent signals, with different behaviour during the rotation of the sample in an in-plane field. The signal observed in the range $|\mathbf{H}| <\sim 10\,\mathrm{mT}$, indicated by a yellow stripe in figure 3(b), changes its sign every 90°. This change of sign is especially clear when we compare scans at $\phi = 70^\circ$ and 135°, i.e. with **H** in the vicinity of the global (biaxial) easy axes. This behaviour is also, as the mentioned above resistance value at $\mathbf{H} = 0\,\mathrm{T}$, very similar to the one observed for the type I anisotropy. The second signal, with the high resistance level limited by positions 5–6, on the other hand, behaves very similarly to the one observed in the case of type II. Specifically, we do not observe a change of sign when the sample is simply rotated by 90°. The only exception is the case of $\phi = 90^\circ$, i.e. when **H** is applied along the hard/HR axis. The field scans and the behaviour of the spin-valve signal then confirm our conclusion from the discussion of the angle scans that the type III anisotropy can be described as the combination of the types I and II with the uniaxial anisotropy superimposed on *both* easy and hard cubic axes.

Having discussed the details of observed spin-valve-like signals, we can now revisit our assumption regarding the high/low resistance–easy/hard magnetic axis correspondence observed for our samples at the saturation field of 1 T. Summarizing the above discussion, we note that there are two main differences in scans measured in the case of type III while comparing it with the type II results: (i) two distinct values of resistance at $\mathbf{H} = 0\,\mathrm{T}$ and (ii) the change of the sign of the spin-valve-like signal while rotating the sample every 90°. Anisotropy types II and III differ only by a non-equivalency of directions characterized by *high resistance* values, observed in the case of type III (figure 2(c)) but not in the case of type II (figure 2(b)). This non-equivalency of *high resistance* directions, on the other hand, is observed also for the type I anisotropy (figure 2(a)), i.e. it is the common feature for type III and type I. We have noted already in the previous paragraph that features (i) and (ii) resemble those observed in the case of sample A, i.e. for the type I anisotropy. We could say then that non-equivalency of *high resistance* directions is responsible for such behaviour of the spin-valve signal. As discussed in the case of type I, those features can be easily explained by uniaxial anisotropy superimposed on biaxial *easy* directions and breaking the perfect cubic symmetry and equivalency of cubic *easy* axes. Therefore, we conclude that high resistance axes are easy magnetic axes also for sample B, i.e. the correspondence high (low) resistance–easy (hard) magnetic axis, as observed at the saturation field of 1 T, is indeed valid for this sample too. This correspondence is valid also for uniaxial easy/hard directions when this type of anisotropy is superimposed on biaxial hard axes. We know that as a result of an uniaxial anisotropy, global easy axes are drawn towards the uniaxial easy axis [13] and in figures 2(b) and (c) we can see how those axes are drawn towards the HR 90° uniaxial axis, when compared with figure 2(a), i.e. the type I anisotropy. Also field scans in figure 3(b) reveal that magnetoresistance curves along this direction are much flatter than along the 0° direction, supporting the claim that this is indeed an easy uniaxial axis.

Let us now briefly discuss the possible origin of different types of observed uniaxial anisotropies. Typically, a (Ga,Mn)As layer grown epitaxially on a GaAs substrate is subjected to compressive strain in the sample. This results in a biaxial in-plane anisotropy with easy axes along [100] and [010] directions [14, 15], as also observed in this study. This cubic-like anisotropy dominates at low temperatures, however an additional uniaxial anisotropy along [110] directions is also observed in the system. Although the microscopic mechanism behind breaking the biaxial symmetry and the equivalence of [110] and [$\bar{1}$10] directions is still not fully understood, the theoretical model employing an extrinsic triagonal distortion along [110] seems to explain the experimental data well [14]. Interestingly, however, according to the results of calculations presented in [10], both the tunnelling current magnitude and its spin polarization in p^+-(Ga, Mn)As/n^+-GaAs Esaki–Zener devices can differ for magnetizations along [110] and [$\bar{1}$10] directions even in the absence of extrinsic distortion. This reflects the asymmetry of the (Ga,Mn)As/GaAs interface at which these two directions are not equivalent. To explain the breaking of the symmetry between [100] and [010] directions, one has to, however, invoke an extrinsic deformation. Because all our samples were fabricated from the same wafer, the presence of different types of the observed uniaxial anisotropy suggests that it is not simply the bulk property of the wafer. We suggest that it could have been introduced into the system during processing of the wafer, as a result of strain modifications. The effect of the processing on the magnetic anisotropy of (Ga,Mn)As seems to be very random for our samples, however, we did not investigate this in detail. There has been a recent report of how the anisotropy could be controlled by lithography-induced strain relaxation [16]. Results for sample B suggest that one has to be cautious, as the anisotropy can be influenced by different conditions of the cooldown. This too could be the result of strain modifications, although also was not investigated by us in detail. Because the processing of our samples included annealing at 250 °C, one should mention the possible influence of this process on the magnetic anisotropy of the samples, i.e. on the results of our experiments. As it was shown in [14], an annealing at temperature close to the growth temperature of the (Ga,Mn)As layer can rotate the uniaxial easy axis from [$\bar{1}$10] to [110] or the other way around. Because the annealing time was, however, very short (5 min) in our case and all our samples were annealed this does not affect our discussion. To summarize, the results of our experiments show that one has to be careful while performing spin-valve experiments with (Ga, Mn)As/n^+-GaAs Zener–Esaki devices, and be aware of the different types of anisotropies that can be present in devices and can influence the measured signal through the TAMR effect.

3. Nanoconstrictions in lateral (Ga,Mn)As

3.1. Introduction

A very large spin-valve-like effect of about 2000% was found by Rüster *et al* [17] in the magnetoresistance across nanoconstrictions in ferromagnetic (Ga,Mn)As wires. The geometry of employed devices was very similar to the one shown in the central panel of figure 4, with the magnetic field aligned along the long axis of the wire. We have already reported on a similar experiment [18] in which we observed an even higher effect for a device structured in a 50 nm thick (Ga,Mn)As epilayer. The effect was explained within the tunnelling magnetoresistance (TMR) picture where the tunnelling occurs across an in-plane barrier due to depletion in the vicinity of the nanoconstrictions. The low resistance state of the spin-valve signal was

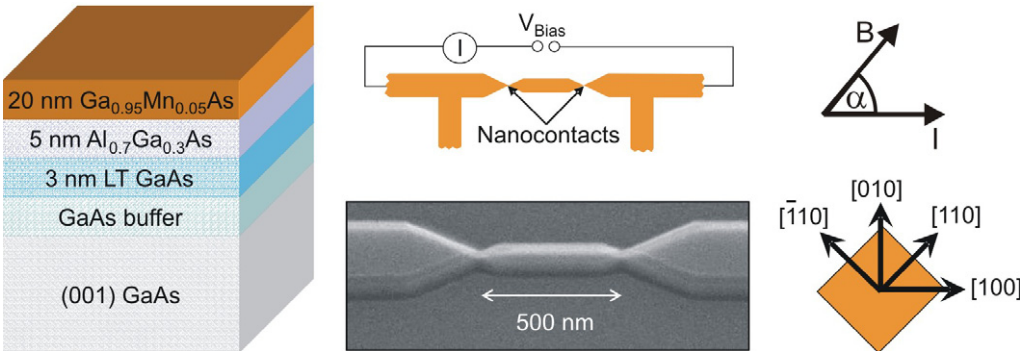

Figure 4. Left: MBE-grown wafer used for processing nanostructures. Middle: schematics and electron micrograph of a (Ga,Mn)As device with nanoconstrictions. Right: crystallographic axes and definition of angle α between external magnetic field **B** and current **I**.

attributed to a parallel alignment of the magnetizations in all three parts of the structure (the two 'leads' and the central island), whereas the high resistance state was attributed to an antiparallel configuration. Giddings *et al* [7] performed similar experiments on a slightly modified structure. Instead of a narrow (Ga,Mn)As island detached by two nanoconstrictions from wider (Ga,Mn)As input leads (as presented here) they investigated a 3 μm wide Hall bar with two constrictions inserted along its length. Therefore, the magnetization of the three parts of the structure was always aligned parallel to each other because of their identical coercive fields. They found surprisingly large effects while varying the direction of an in-plane magnetic field and hence the in-plane magnetization. The sign of the 'TMR-like' effect observed in this experiment switched with the magnetic field direction. As this excludes the conventional TMR effect as the origin of the observed spin-valve-like signal, the TAMR picture [1] was employed as an explanation, since the signal could be inverted by a 90°-rotation of the external magnetic field with respect to current. As in vertical tunnelling devices the TAMR effect is ascribed to an anisotropic density of states of the holes in the valence band of (Ga,Mn)As which varies with the magnetization direction. Using the Landauer transmission probabilities at the Fermi energy, theoretical TAMR values between ∼50% and ∼1% were estimated for hole densities $0.1–1 \times 10^{20}\,\mathrm{cm}^{-3}$ [7].

Here, we present angle-, bias- and temperature-dependent magnetoresistance measurements on a double constricted (Ga,Mn)As tunnelling structure (figure 4). The magnetoresistance effects described below are much larger than observed before and exclude a straightforward explanation in the picture of TMR and TAMR alone.

3.2. Experimental details

3.2.1. Sample preparation. The devices investigated here were made from wafers grown by MBE. The layer sequence is shown in figure 4. As a substrate, we used (001)-GaAs. 20 nm thick $Ga_{0.95}Mn_{0.05}As$ was grown by LT MBE at $T = 243°C$ on top of 5 nm $Al_{0.7}Ga_{0.3}As$, 3 nm LT GaAs and a GaAs buffer layer. After annealing a Curie temperature of about 99 K and a carrier density of about $1.8 \times 10^{20}\,\mathrm{cm}^{-3}$ was achieved. The wafer was then pre-patterned with a Hall bar structure using optical lithography and chemical wet etching. After short ion-beam etching with Ar ions to remove oxide layers, Au contacts were defined by a standard lift-off method.

For nanopatterning, we used electron beam lithography with PMMA (polymethyl methacrylate) as a negative resist followed by $SiCl_4$-based RIE. A schematic and an electron micrograph of a typical sample is shown in the central panel of figure 4. The central island is 500 nm long and 100 nm wide. The outer wires are about 10 μm long and 400 nm wide. To enter the lateral tunnelling regime, the constriction width has to be less than 30 nm. The formation of a barrier is ascribed to the reduction of the carrier density due to surface depletion [17].

3.2.2. Measurements. Magnetotransport measurements were carried out in a ^{4}He bath cryostat with a superconducting magnet. The temperature of the measurements was 4.2 K, unless mentioned otherwise. The angle α between an external in-plane magnetic field and the current direction could be varied by rotating the sample holder. Two types of measurements are presented below. For field scans the angle α was fixed and the magnetic field was swept from -100 mT to +100 mT. Before each sweep, the sample was magnetized to saturation by applying 1 T. In order to check the reproducibility, we always took the up- and down-sweep. The second type of measurement, the angle scan, was performed in a high magnetic field of 5 T. In this case, the magnetization vector in each part of the structure follows the external field orientation and hence the magnetization in the leads and the island is always parallel. All electrical measurements were performed using dc technique in a 2-point configuration. A constant voltage V_{bias} was applied along the wire ([100] easy direction) and the resulting current I was measured using a current amplifier.

3.3. Results and discussion

Figure 5 shows the magnetoresistance for different angles α of a tunnel device with a constriction width $<$30 nm. If the magnetic field is oriented along the current direction ($\alpha = 0^\circ$) and swept, e.g. from negative to positive values, a huge jump from a low to a high resistance state and back is observed. This behaviour was ascribed before to TMR due to parallel and antiparallel magnetization configurations [17]. The aspect ratio (width/length) of the (Ga,Mn)As island in comparison to the outer parts (see figure 4) leads to different coercive fields which could explain the spin-valve-like signal. Rotating the sample brings, however, a more complex behaviour. A clear spin-valve-like signal occurs between $0^\circ \ldots 45^\circ$ and $165^\circ \ldots 180^\circ$. The size of the effect, as well as the absolute values for the high- and low-resistance states vary only marginally in this range. Between $\alpha = 135^\circ$ and $\alpha = 150^\circ$ a typical spin-valve-like signal is observable but the value of the high resistance state is reduced. For the other angles, it is difficult to link the resistance behaviour to different magnetization configurations. For $\alpha = 75^\circ$, the negative MR cannot be explained by the TMR since the high resistance state occurs at high fields. There, however, one would expect a parallel magnetization configuration and hence a low resistance state. From the data displayed in figure 5, we have to conclude that other mechanisms are at work. The change of the sign of the spin-valve-like signal points to TAMR.

To investigate the TAMR contribution, we applied a strong in-plane magnetic field of 5 T which aligns all magnetization vectors parallel to each other along the external B-field direction. Under these conditions the anisotropic behaviour of the longitudinal resistance could be detected and results are shown in figure 6. These data were obtained for the same sample as the data in figure 5, on a different cooldown, however. At this point one has to mention that although the size of the effects can change significantly after thermal cycling, the angular-, bias voltage- and temperature-behaviour remains essentially the same. The colourscale of the

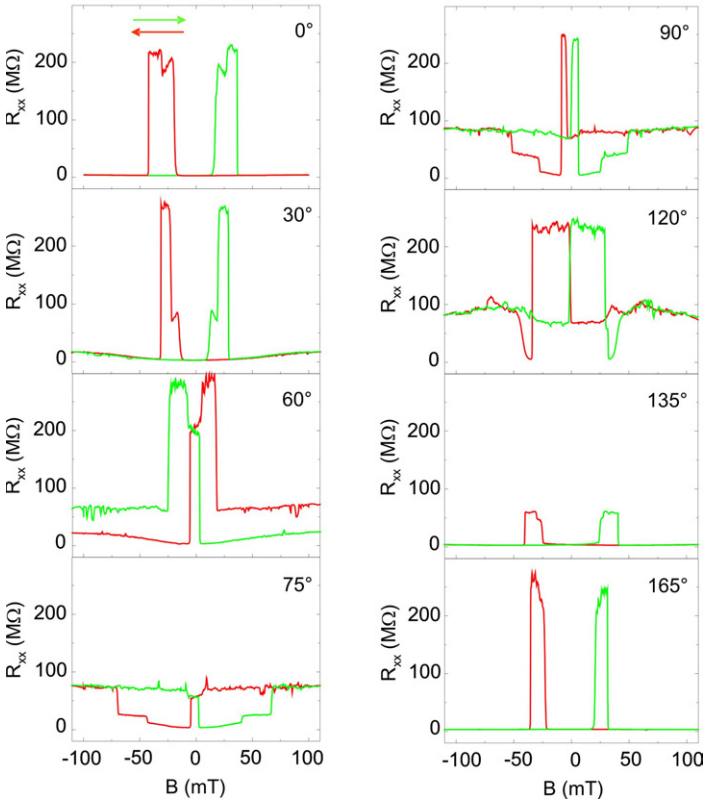

Figure 5. Magnetoresistance at $T = 4.2\,\mathrm{K}$ and $V_{\mathrm{Bias}} = 3\,\mathrm{mV}$ for different angles α. Magnetic field sweeps in positive (green colour) and negative (red) directions are shown.

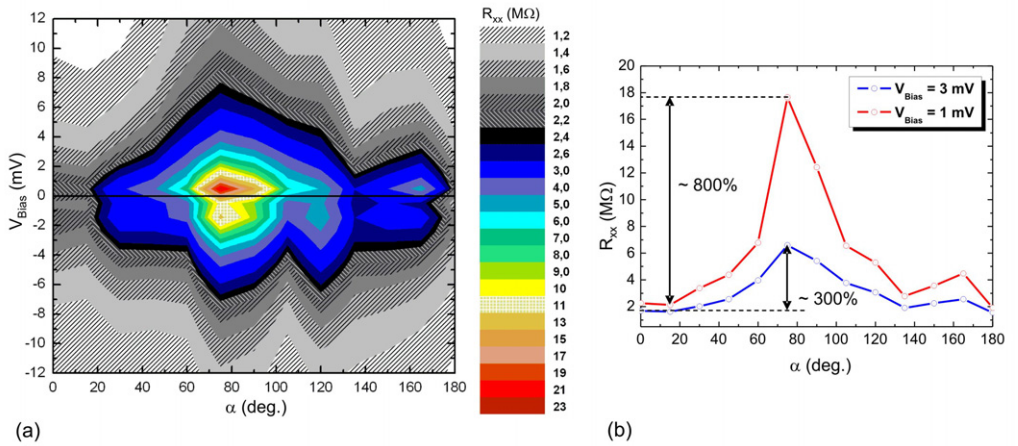

Figure 6. (a) Colour plot of the longitudinal resistance R_{xx} dependence on bias voltage V_{Bias} and angle α at 4.2 K. To exclude the TMR a high magnetic field of $B = 5\,\mathrm{T}$ was applied for these measurements. (b) Anisotropic resistance behaviour at 4.2 K and $B = 5\,\mathrm{T}$ for a constant bias voltage of 1 and 3 mV.

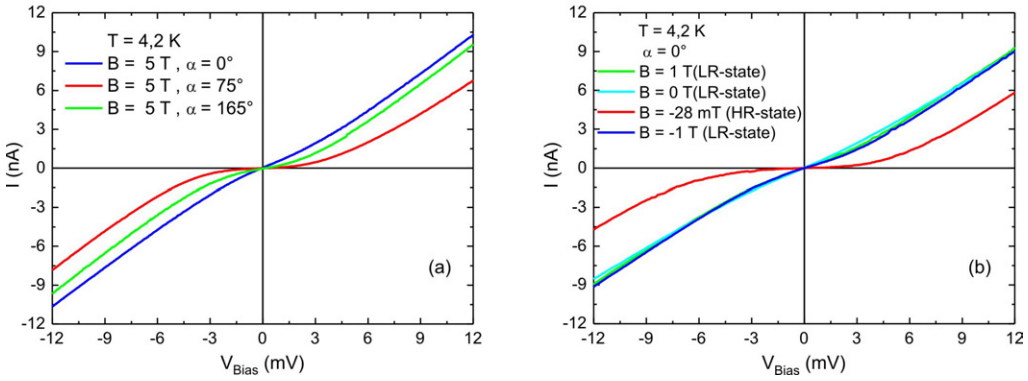

Figure 7. (a) I–V characteristics for three different magnetization orientations (angles α) at $T = 4.2$ K and $B = 5$ T. (b) I–V characteristics for the LR and HR state during a magnetic reversal process at $T = 4.2$ K and $\alpha = 0^\circ$.

magnetoresistance is plotted in figure 6(a) as a function of the angle α (in 15° steps) and bias voltage V_{bias}. A distinct maximum is found at $\alpha = 75^\circ$. Particularly for bias voltages below 2 mV the resistance rises strongly around $\alpha = 75^\circ$. For small angles up to 20° the resistance remains consistently low, even at small bias voltages. In figure 6(b), the longitudinal resistance R_{xx} is plotted versus α for $V_{\text{Bias}} = 3$ mV and $V_{\text{Bias}} = 1$ mV. A maximum TAMR effect of 300 and 800% is observed, respectively. This effect seems to be much too high to be explained on the basis of an anisotropic density of states alone where a maximum of 50% is expected [7]. Also the TMR effect can be excluded as the magnetization on both sides of the constriction is forced into the same direction by the strong applied B-field. In figure 7(a), we plot the I–V characteristics across the island for three different angles α in the in-plane B-field of 5 T. The I–V characteristics, i.e. the degree of nonlinearity and hence the barrier height strongly depend on the direction of the magnetization. For $\alpha = 0^\circ$ the I–V characteristic is nearly linear while for $\alpha = 75^\circ$, it is strongly nonlinear. A similar angular dependence was found in the case of constrictions with different anisotropies on both sides of the neck [20]. Such a type of I–V behaviour can be found at certain magnetic field values during magnetization reversal. As an example, we plot in figure 7(b) I–V curves for $\alpha = 0^\circ$ and 4.2 K obtained at four different values of magnetic field. At $B = -1$T, $B = 0$ T and $B = 1$ T the device is in a LR state while at $B = -28$ mT it is a HR state (see figure 5). While the I–V characteristic is quite linear for the LR state, it shows a strong nonlinearity in the HR state. This suggests that the latter is associated with a magnetization orientation, at least in the vicinity of the nanoconstriction(s), which is strikingly different from the direction of the external B-field. Hence, the picture in which the large magnetoresistance effect for this orientation is solely due to tunnelling between parallel or antiparallel oriented regions of magnetization on both sides of the constriction [17] seems not to be sufficient. The different I–V characteristics for different magnetization directions suggest that the height of the tunnelling barrier itself must depend on the magnetization direction. Such a scenario would also be consistent with the strong temperature and bias dependence, shown in figure 8. The effect increases strongly by decreasing bias voltage (figure 8(a)) or decreasing temperature (figure 8(b)). Raising, for example, the bias voltage from 1 to 3 mV reduces the effect from about 14 000 to 6500% at 4.2 K and $\alpha = 0^\circ$ (figure 8(a)). At a constant bias voltage of 3 mV the MR-effect increases from about 40% at 30 K to about 9500% at 1.4 K

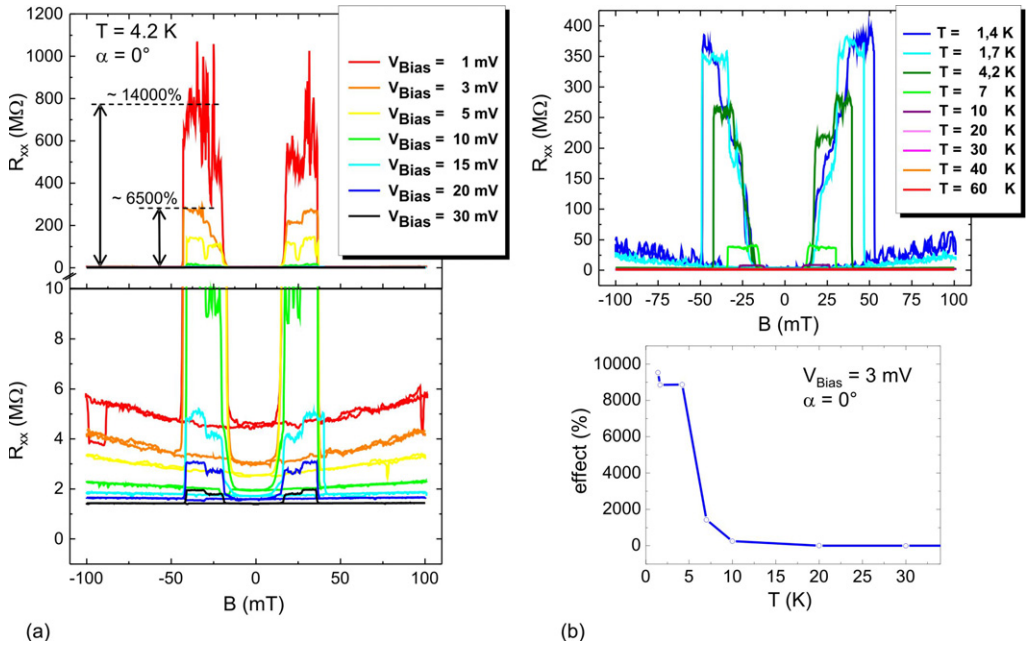

Figure 8. (a) Bias voltage dependence of the spin-valve-like MR at $T = 4.2\,\mathrm{K}$ and $\alpha = 0^{\circ}$. (b) Temperature dependence of the MR-effect at $V_{\mathrm{Bias}} = 3\,\mathrm{mV}$ and $\alpha = 0^{\circ}$.

(figure 8(b)). While the switching fields are independent of the bias voltage they are shifted by temperature. This is likely due to the competition of two anisotropy contributions, namely the strain induced uniaxial anisotropy and the crystallographic cubic anisotropy that are influenced by temperature [15]. The strong temperature and bias dependence of the effect as well as the angular anisotropic *I*–*V* characteristic might be associated with a magnetization dependent metal–insulator transition. As the carrier density is expected to be reduced in the vicinity of the constriction, the system is closer to the metal–insulator transition and such a scenario seems consistent with the observations. A similar explanation was put forward recently to explain the huge magnetoresistance effects in vertical (Ga,Mn)As/GaAs/(Ga,Mn)As tunnel junctions [19] and nonlinear *I*–*V* traces in constrictions with different anisotropies [20]. Alternatively, the observed phenomena might be due to Coulomb-blockade where charge carriers tunnel in and out of nanoscale metallic islands embedded in a tunnel barrier formed by the constriction. That the Coulomb-blockade, and hence the resistance, strongly depend on the magnetization direction has been shown recently [21]. More experiments are needed to resolve which effect is the dominating one in transport through nanoconstrictions in (Ga,Mn)As.

4. Summary

We have presented here the results of our magnetotransport experiments on two types of (Ga,Mn)As-based tunnel devices: vertical p^{+}-(Ga, Mn)As/n^{+}-GaAs Esaki diodes and laterally defined nanoconstrictions in (Ga,Mn)As epilayers. Both types of devices exhibited features related to the novel tunnelling anisotropic magnetoresistance effect, namely gradual changes of magnetoresistance with the rotation of the in-plane magnetization of the magnetic material

and the reversal of the related spin-valve-like signal upon rotation in the in-plane magnetic field. The results of the experiments on Esaki diode devices could be satisfactorily explained by the TAMR picture alone. The measurements revealed three different magnetic anisotropy types observed for different devices. These affected strongly the resulting spin-valve like signal, that could switch its sign by a simple rotation by 90°or not, depending on whether a uniaxial anisotropy is superimposed on, respectively, easy or hard axes of the dominant crystallographic biaxial anisotropy. This suggests that a careful approach should be taken while interpreting the results of any spin-injection experiments with (Ga, Mn)As/n^+-GaAs Esaki diodes in a spin-valve configuration.

The TAMR picture alone was not enough, however, to explain the results of magneto-transport experiments on nanoconstricted (Ga,Mn)As wires, as the size of the effect seemed to be too high to be explained on the basis of an anisotropic density of states. For one part, the traditional TMR effect cannot be completely excluded from the explanation. Current–voltage characteristics, measured for different angles between the current and the applied field, suggested however, that a magnetization dependent metal–insulator transition or Coulomb blockade may play a significant role in the observed magnetoresistance effects.

Acknowledgments

This research was supported by a Marie Curie Intra-European Fellowship within the 6th European Community Framework Programme and by Collaborative Research Centre SFB 689 of the German Science Foundation.

References

[1] Gould C, Rüster C, Jungwirth T, Girgis E, Schott G M, Giraud R, Brunner K, Schmidt G and Molenkamp L W 2004 Tunneling anisotropic magnetoresistance: a spin-valve-like tunnel magnetoresistance using a single magnetic layer *Phys. Rev. Lett.* **93** 117203

[2] Cowburn R P, Gray S J, Ferre J, Bland J A C and Miltat J 1995 Magnetic switching and in-plane uniaxial anisotropy in ultrathin Ag/Fe/Ag(100) epitaxial films *J. Appl. Phys.* **78** 7210

[3] Tang H X, Kawakami R K, Awschalom D D and Roukes M L 2003 Giant planar Hall effect in epitaxial (Ga,Mn)As devices *Phys. Rev. Lett.* **90** 107201

[4] Rüster C, Gould C, Jungwirth T, Sinova J, Schott G M, Giraud R, Brunner K, Schmidt G and Molenkamp L W 2005 Very large tunneling anisotropic magnetoresistance of a (Ga,Mn)As/GaAs/(Ga,Mn)As stack *Phys. Rev. Lett.* **94** 027203

[5] Giraud R, Gryglas M, Thevenard L, Lemaître A and Faini G 2005 Voltage-controlled tunneling anisotropic magnetoresistance of a ferromagnetic p^{++}-(Ga, Mn)As/n^+-GaAs Zener-Esaki diode *Appl. Phys. Lett.* **87** 242505

[6] Moser J, Matos-Abiague A, Schuh D, Wegscheider W, Fabian J and Weiss D 2007 Tunneling anisotropic magnetoresistance and spin-orbit coupling in Fe/GaAs/Au tunnel junctions *Phys. Rev. Lett.* **99** 056601

[7] Giddings A D *et al* 2005 Large tunneling anisotropic magnetoresistance in (Ga,Mn)As nanoconstrictions *Phys. Rev. Lett.* **94** 127202

[8] Kohda M, Ohno Y, Takamura F and Ohno H 2001 A spin Esaki diode *Japan. J. Appl. Phys.* **40** L1274
Johnston-Halperin E, Lofgreen D, Kawakami R K, Young D K, Coldren L, Gossard A C and Awschalom D D 2002 Spin-polarized tunneling in (Ga,Mn)As *Phys. Rev.* B **65** 041306

[9] Van Dorpe P, Liu Z, Van Roy W, Motsnyi V F, Sawicki M, Borghs G and De Boeck J 2004 Very high spin polarization in GaAs by injection from a (Ga,Mn)As Zener diode *Appl. Phys. Lett.* **84** 3495–7

[10] Sankowski P, Kacman P, Majewski J A and Dietl T 2007 Spin-dependent tunnelling in modulated structures of (Ga,Mn)As *Phys. Rev.* B **75** 045306
[11] Ciorga M, Einwanger A, Sadowski J, Wegscheider W and Weiss D 2007 Tunneling anisotropic magnetoresistance effect in a p^+ -(Ga,Mn)As/n^+-GaAs Esaki diode *Phys. Status Solidi* a **204** 186
[12] Pappert K, Hümpfner S, Wenisch J, Brunner K, Gould C, Schmidt G and Molenkamp L W 2007 Transport characterization of the magnetic anisotropy of (Ga,Mn)As *Appl. Phys. Lett.* **90** 62109
[13] Daboo C, Hicken R J, Eley D E P, Gester M, Gray S J, Ives A J R and Bland J A C 1994 Magnetization reversal processes in epitaxial Fe/GaAs(001) films *J. Appl. Phys.* **75** 5586
[14] Sawicki M *et al* 2005 In-plane anisotropy rotations in (Ga,Mn)As thin films *Phys. Rev.* B **71** 121302
[15] Wang K Y, Edmonds K W, Campion R P, Zhao L X, Foxon C T and Gallagher B L 2005 Anisotropic magnetoresistance and magnetic anisotropy in high-quality (Ga,Mn)As films *Phys. Rev.* B **72** 085201
[16] Wenisch J, Gould G, Ebel L, Pappert K, Schmidt M J, Kumpf C, Schmidt G, Brunner K and Molenkamp L W 2007 Control of magnetic anisotropy in (Ga,Mn)As by lithography induced strain relaxation *Preprint* cond-mat/0701479
Hümpfner S, Pappert K, Wenisch J, Brunner K, Gould C, Schmidt G, Molenkamp L W, Sawicki M and Dietl T 2007 Lithographic engineering of anisotropies in (Ga,Mn)As *Appl. Phys. Lett.* **90** 102102
[17] Rüster C, Borzenko T, Gould C, Schmidt G and Molenkamp L W 2003 Very large magnetoresistance in lateral ferromagnetic (Ga,Mn)As wires with nanoconstrictions *Phys. Rev. Lett.* **91** 216602
[18] Schlapps M, Doeppe M, Wagner K, Reinwald M, Wegscheider W and Weiss D 2006 Transport through (Ga,Mn)As nanoconstrictions *Phys. Status Solidi* a **203** 3597
[19] Pappert K, Schmidt M J, Hümpfner S, Rüster C, Schott G M, Brunner K, Gould C, Schmidt G and Molenkamp L W 2006 Magnetization-switched metal-insulator transition in a (Ga,Mn)As tunnel device *Phys. Rev. Lett.* **97** 186402
[20] Pappert K, Hümpfner S, Gould C, Wenisch J, Brunner K, Schmidt G and Molenkamp L W 2007 Exploiting locally imposed anisotropies in (Ga,Mn)As: a non-volatile memory device *Preprint* cond-mat/0701478
[21] Wunderlich J, Jungwirth T, Irvine A C, Kaestner B, Shick A B, Campion R P, Williams D A and Gallagher B L 2007 Coulomb blockade anisotropic magnetoresistance and voltage controlled magnetic switching in a ferromagnetic GaMnAs single electron transistor *J. Magn. Magn. Mater.* **310** 1883